

Article

Effect of Masonry Infill Constitutive Law on the Global Response of Infilled RC Buildings

Marco Gaetani d'Aragona , Maria Polese * and Andrea Prota

Department of Structures for Engineering and Architecture, University of Naples Federico II, Via Claudio 21, 80125 Naples, Italy; marco.gaetanidaragona@unina.it (M.G.d.); aprota@unina.it (A.P.)

* Correspondence: maria.polese@unina.it

Abstract: Masonry-infilled reinforced concrete frames represent a very common construction typology across the Mediterranean countries. The presence of infills substantially modifies the global seismic performances of buildings in terms of strength, stiffness, and energy dissipation. Although several research studies focused on the overall performances of infilled reinforced concrete frames, the modeling of infill panels remains an open issue due to the complex interaction between the infill and the frame and the uncertainties involved in the definition of the problem. In the present paper, an existing masonry-infilled RC frame designed according to obsolete seismic codes is chosen as a case study. A refined three-dimensional finite element model is built for performing nonlinear static and time-history analyses in order to investigate some significant aspects related to the modeling of infills. In particular, it is investigated the effect of different infill constitutive models on the seismic performance of infilled RC building expressed in terms of engineering demand parameters such as interstorey drift ratios and peak floor accelerations, and on the generation of damage fragility curves.

Keywords: infilled frames; nonlinear time-history; seismic capacity; damage state fragility curves; interstorey drift ratios; peak floor acceleration



Citation: Gaetani d'Aragona, M.; Polese, M.; Prota, A. Effect of Masonry Infill Constitutive Law on the Global Response of Infilled RC Buildings. *Buildings* **2021**, *11*, 57. <https://doi.org/10.3390/buildings11020057>

Academic Editor: Humberto Varum
Received: 29 December 2020
Accepted: 31 January 2021
Published: 7 February 2021

Publisher's Note: MDPI stays neutral with regard to jurisdictional claims in published maps and institutional affiliations.



Copyright: © 2021 by the authors. Licensee MDPI, Basel, Switzerland. This article is an open access article distributed under the terms and conditions of the Creative Commons Attribution (CC BY) license (<https://creativecommons.org/licenses/by/4.0/>).

1. Introduction

Reinforced concrete (RC) buildings infilled with masonry panels represent a relevant portion of the existing building stock across the Mediterranean countries [1,2]. According to the current construction practice, infill panels are encased between framing members significantly influencing the structural response under seismic loadings. Observations from past earthquakes demonstrate that masonry infill walls often behave as primary structural elements [3]. The distribution in plan and elevation of masonry panels strongly influences the behavior of the building at the global level leading to an increase of structure lateral stiffness [4–6], strength [7,8], and energy dissipation, and strongly affecting the seismic performances and the collapse mechanism [9] of the structures, and the building residual capacity [10–13]. Further, the presence of an irregular infill layout may lead to additional torsional effects or the development of soft-story mechanisms [14], while a regular layout contributes to the reduction of lateral deformations [6]. Even in presence of a regular layout, the abrupt failure of some panels during an earthquake may lead to modification of the geometrical configuration with a sudden manifestation of the mentioned effects. Moreover, the interaction between infills and the surrounding frame significantly influences the building behavior at the local level leading to a modification of internal force distributions that may trigger the activation of brittle collapse mechanisms at the RC member extremities [15–17]. The contribution of infill panels depends on a series of geometric and mechanical features of the masonry infills and the surrounding frame. Material, consistency, and opening percentage of infill panels are extremely variable across the whole Mediterranean countries depending on the material availability, construction techniques, and environmental conditions.

Due to the significant contribution of masonry infills to the seismic performances of RC frames both at the local and global level, the modeling of infill panels represents a crucial aspect when the actual building response under cyclic actions needs to be reproduced. Although the actual role of infills on the lateral response of buildings is widely recognized, different modeling approaches have been proposed and developed to account for the infill contribution and interaction with the surrounding frame, and there is still a lack of well-established and reliable analytical models for the simulation [18,19].

Most refined methods, such as micro-modeling approaches, are based on a finite element representation of frame and infills and require an accurate definition of constitutive relationships describing the cyclic behavior of bricks and mortar joints. These modeling approaches have the advantage of allowing to capture the development of local phenomena. However, due to a large amount of information and the remarkable computational effort required, the adoption of simpler methods is generally preferred. In particular, the so-called macro-modeling approach that employs equivalent struts is one of the most adopted in the numerical analysis of infilled frames and widely used in loss estimation frameworks [9,20] or to generate mechanical-based fragility curves [21]. Different approaches are available in the literature depending on the number, the geometrical configuration of the equivalent struts, and the constitutive models describing the cyclic behavior of infill panels. Depending on the mechanical model and the response envelope adopted, the results in terms of building response may significantly vary [19].

The choice of the most appropriate analytical model to be used for the assessment of masonry-infilled RC buildings is of paramount importance when the global building performances have to be estimated, especially in terms of damage and repair costs. In fact, the adoption of alternative constitutive models to simulate the presence of infill panels may lead to a different distribution of deformations and accelerations along the height, possibly affecting the distribution and amount of damage and leading to different collapse modes. While several authors studied the static cyclic response of single-bay single-story frames, often focusing on the comparison between the results via analytical models and experimental tests (e.g., [9,19]), very few studies focused on the effect of different infill modeling approaches on the global seismic performances of buildings under dynamic loadings. Based on these considerations, further research is still required to provide extensive indications to account for the response of masonry infills. To this scope, this paper investigates the effect of the adopted infill constitutive model on the building response in terms of engineering demand parameters, which are directly related to damage and repair costs, for a case study building.

In the present study, an existing masonry-infilled RC frame constructed according to obsolete seismic code provisions is considered as a case study. Three different strut backbone curves are employed and the effect of the infill model on the global seismic performances of RC buildings is analyzed. Static pushover and incremental dynamic analyses are performed on a refined three-dimensional model adopting a ground motion bin consisting of 42 records in order to deduce some critical observations about the dependence of the building seismic performances on the infill model. The comparative analysis allowed us to investigate the role of the strut backbone curve of the infill on the seismic behavior of RC frames in terms of attainment of damage states, distribution of interstory drift ratios, and peak floor accelerations. Section 2 introduces the most common techniques to explicitly model the contribution of the infill panel. Focusing on the single-strut modeling approach and with reference to the different backbone curves adopted in this study, the assumptions regarding the strut hysteretic behavior and the geometrical and mechanical characterization are introduced. Section 3 presents the research methodology. Section 4 introduces the case-study building and describes the refined three-dimensional finite element model. In Section 5, the influence of the infill backbone curve is analyzed in terms of static response, while in Section 6 the influence of the infill backbone curve on the seismic performances of the building is analyzed in terms of damage intensity and distribution along the height.

2. Modeling Approaches to Simulate the Presence of Masonry Infills

2.1. Micro- and Macro-Modeling Approaches

In the scientific literature, several modeling techniques were proposed to simulate the infill-frame interaction, which can be grouped into micro- [22,23] and macro-modeling [24–26] approaches.

Micro-modeling strategies can be further subdivided into detailed and simplified approaches [27,28]. The detailed approach simulates the behavior of the masonry panel by means of discrete brick units and the brick-mortar interaction is represented by different continuum elements, while in the simplified approach bricks and mortars are condensed into a common element. Micro-models represent the most accurate strategy to capture infill-frame interaction, being able to capture the real physics of the problem such as the stiffening effect, the sliding of the brick units along the mortar joints, the crack propagation, and the local effects induced by masonry on the surrounding frame. However, these models present a double difficulty requiring a proper calibration of a large number of parameters and a high computational effort. For these reasons, the use of micro-modeling approaches is generally limited to specific research scopes.

Mechanic-based macro-modeling approaches are derived based on the observation from experimental test results where the load path within the infill panel mainly follows the diagonal direction [29–31]. The idea behind the macro-modeling approach is to replace masonry infills by means of one or more equivalent pin-jointed struts for each panel. This technique is largely adopted by engineers and researchers due to its simplicity in implementation and the low computational effort required. However, despite the adoption of the equivalent strut is quite effective and simple, it presents a number of crucial aspects that, if not properly managed, may compromise the quality of obtained results since the macro-model should be able to account for strength, stiffness, and damage evolution in a proper way. In particular, the definition of the equivalent strut requires the assignment of mechanical parameters that depend on the properties of the actual system, and that for existing buildings is affected by large uncertainties related not only to masonry properties but also to manufacturing and arrangement details.

Due to large uncertainties affecting the definition of macro-models, several solutions were proposed in past studies, in which the fundamental factors governing the definition of equivalent strut model may significantly differ. In particular, these factors consist of the number of equivalent struts, the width, and constitutive relationship for the struts.

Depending on the modeling strategy, the number of element simulating the masonry panel can range from single (e.g., [32]) to multiple (e.g., [33,34]) struts. The single strut model is largely adopted by practitioners due to its flexibility and simplicity of use. Further, the model is able to provide a good approximation of the global building response despite its simplicity. However, the main limit of this model is that it adopts a concentric position for the equivalent strut that does not allow us to properly account for shear force transmission in surrounding RC members. In existing RC buildings, which are often characterized by the presence of non-ductile members and non-seismic details, these additional shear forces produced by the infill-frame interaction may lead to premature triggering of brittle failures at the top of the columns or in beam-column joint panels. To overcome this issue, more complex macro-models were developed employing multiple diagonal struts. Different prescriptions regarding the number, the inclination, and the point with surrounding RC frame are provided in literature and need to be adequately calibrated. In this case, the model is affected by uncertainties arising from the calibration of constitutive laws for each strut, especially when performing nonlinear analyses. In some cases, the constitutive laws assigned to multiple struts can be the same as the case for the single one. So, the choice of the amount in terms of transversal section dimension and of stiffness shared among the struts need to be assigned to single struts, and it is not univocal (e.g., [35,36]) and affects the final response of the structure.

2.2. Single-Strut Model

The single-strut model is widely adopted by engineers and researchers since it provides a good compromise between simplicity and accuracy in predicting analytical response. The model involves the replacement of each masonry infill through two opposite diagonal pin-joints struts. Each strut should be able to reproduce with an adequate degree of approximation the damage evolution in terms of stiffness and strength when performing nonlinear static or dynamic analyses. The identification of the equivalent diagonal strut requires the assignment of specific mechanical properties that, for existing buildings, is affected by large uncertainties related not only to masonry properties but also to manufacturing and arrangement details. The main parameters characterizing the masonry strut model are the geometry and constitutive law shape for the masonry strut.

2.3. Single-Strut Geometry

The geometry of the single-strut model varies depending on the relative position of the strut with respect to the main diagonal connecting opposite nodes. For instance, Bertoldi et al. [37], Panagiotakos and Fardis [38], Dolšek and Fajfar [7], Asteris et al. [39], among others, adopt a single compression strut for each direction in a concentric position. Conversely, Zarnic and Tomazevic [40,41] proposed an off-diagonal model in order to account for possible failure induced by infills at the top of the columns. When a concentric position is adopted, the geometry of the diagonal strut is identified by the diagonal length of the strut d_w , determined by the clear length and height of the panel, l_w and h_w respectively, and the equivalent strut width b_w (see Figure 1).

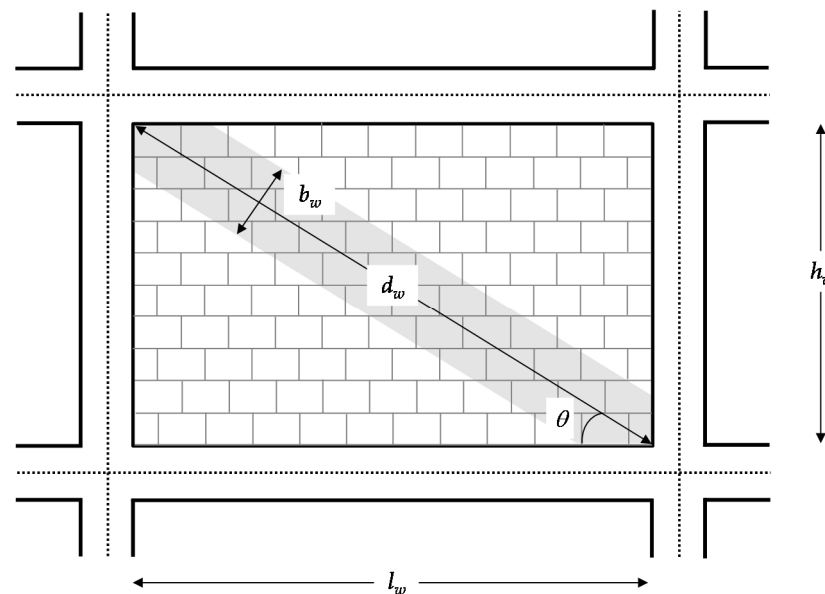


Figure 1. Infill geometric notations adopted in this study.

The single-strut model was originally proposed by Polyakov [42] and implemented by Holmes [32], which proposed to calculate the width of the equivalent strut as 1/3 of the diagonal length. Afterwards, several authors [29–31,37,43–47] proposed more detailed formulations mainly based on the relative infill panel to surrounding frame elastic stiffness λ_h first introduced by Stafford-Smith [29].

2.3.1. Single-Strut Constitutive Law

In order to perform nonlinear analyses of masonry-infilled RC frames, reliable constitutive law describing the equivalent strut in-plane behavior needs to be selected. The constitutive law for a single equivalent strut is generally described by means of a multi-linear relationship calibrated on experimental data as backbone curve for simulating both

the monotonic and the cyclic response. Between the constitutive model proposed in the literature, here three alternative constitutive laws are analyzed in detail: Bertoldi et al. [37], De Risi et al. [48], Huang et al. [49].

The model by Bertoldi et al. [37] adopts a four-branches backbone curve (Figure 2a) for the lateral force-displacement (F-D) relationship. The first ascending branch represents the un-cracked behavior up to the first cracking and the second branch corresponds to the post-cracking behavior up to the development of the peak strength (F_{peak}). The descending third branch of the backbone curve defines the post-peak strength deterioration up to the residual strength (F_{res}). The fourth branch is horizontal and corresponds to the residual strength of the infill panel. The main parameters required to calibrate the proposed model are the width of the equivalent strut (b_w), the secant stiffness at the complete cracking stage (K_{sec}), and the infill panel peak strength (F_{peak}). All the parameters can be defined as a function of the geometric and mechanical characteristics of the infill panel and the surrounding frame.

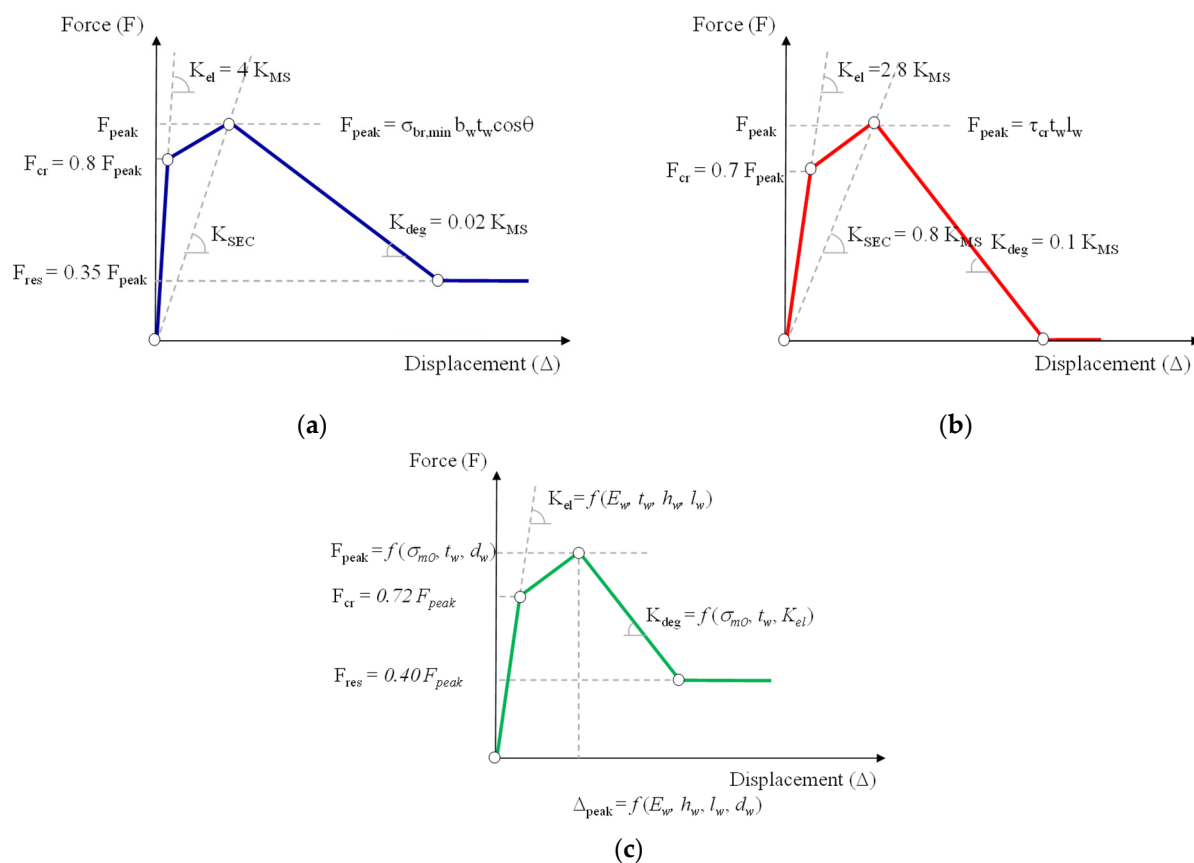


Figure 2. Backbone curves analyzed in this study: adapted from (a) Bertoldi et al. [37], (b) De Risi et al. [48], (c) Huang et al. [49].

The model proposed by Bertoldi et al. [37] is the only one that predicts and explicitly accounts for the failure mode that is likely to be exhibited by the infill panel. In fact, the maximum strength of the panel depends on the predicted failure mode defined based on the infill mechanical properties and corresponds to the minimum among four failure modes. In particular, the peak strength F_{peak} is calculated considering four possible failure modes and the corresponding failure stresses: (a) Diagonal tension, σ_{br1} ; (b) Sliding shear, σ_{br2} ; (c) corner crushing, σ_{br3} ; and (d) diagonal compression, σ_{br4} . The failure stress depends

on the shear strength (τ_{m0}), the bed joints sliding strength (τ_0), the masonry compressive strength (σ_{m0}) and the vertical stress acting on the infill (σ_0):

$$\sigma_{br,1} = \frac{0.6\tau_{m0} + 0.3\sigma_0}{b_w/d} \quad (1)$$

$$\sigma_{br,2} = \frac{(1.2 \sin \theta + 0.45 \cos \theta)\tau_0 + 0.3\sigma_0}{b_w/d} \quad (2)$$

$$\sigma_{br,3} = \frac{(1.12 \sin \theta \cos \theta)}{K_1(\lambda_h)^{-0.12} + K_2(\lambda_h)^{0.88}} \sigma_{m0} \quad (3)$$

$$\sigma_{br,3} = \frac{1.16\sigma_{m0}tg\theta}{K_1 + K_2\lambda_h} \quad (4)$$

where d and θ are the equivalent strut length and inclination, respectively. The term λ_h is a non-dimensional parameter that depends on relative infill panel to surrounding frame elastic stiffness, K_1 and K_2 are two constants calibrated on experimental tests that depends on λ_h [44]. Finally, b_w is the equivalent strut width that is calculated as follows:

$$b_w = \left(\frac{K_1}{\lambda_h} + K_2 \right) d_w \quad (5)$$

The parameter λ_h is defined according to Stafford-Smith [29] as follows:

$$\lambda_h = \sqrt[4]{\frac{E_w t_w \sin(2\theta)}{4EI_c h_w}} h \quad (6)$$

where E_w is the elastic modulus of the infill masonry, EI_c is the product between the elastic modulus of the concrete and the moment of inertia of the columns of the surrounding frame, h_w is the height of the masonry panel, and h is the interstory height.

The secant-to-peak lateral stiffness (K_{sec}) for the equivalent strut is calculated as:

$$K_{sec} = \frac{E_w t_w b_w}{d_w} \cos^2 \theta \quad (7)$$

The remaining parameters required for the definition of the backbone curve are evaluated according to De Sortis et al. [50]. In particular, the cracking-to-peak (F_{cr}/F_{peak}) and the residual-to-peak (F_{res}/F_{peak}) strength ratios are assumed equal to 0.8 and 0.35, respectively. And the cracking-to-peak (K_0/K_{sec}) and the softening-to-peak (K_{deg}/K_{sec}) stiffness ratios are defined as 4.0 and -0.02 , respectively.

Another commonly adopted constitutive model is the modified version of the constitutive law originally proposed by Panagiotakos and Fardis [38]. In the original model, the backbone curve is represented by four branches. Conceptually, the four-branch backbone accounts for different stress states: (a) initial behavior of the un-cracked panel; (b) post-cracked linear response, characterized by a reduction of lateral stiffness due to the detachment of the infill from the surrounding frame; (c) post-peak softening response; (d) achievement of the residual axial strength at a given displacement value. The model by Panagiotakos and Fardis [38] is one of the most widely used in the context of single-strut models for engineering applications. However, it was calibrated on the basis of 10 tests performed on infilled RC frames with hollow masonry bricks that mainly exhibited diagonal cracking failure. For this reason, based on the analysis of a large database of masonry infills made of hollow clay bricks collected to be representative of the Mediterranean building stock, recently De Risi et al. [48] modified the values of the lateral response curve in order to reduce the dispersion when compared to the assembled database. In particular, the cracking (F_{cr}) and peak (F_{max}) strength, the initial un-cracked stiffness (K_0) the cracking-to-peak (K_0/K_{sec}) and the softening-to-peak (K_{deg}/K_{sec}) stiffness ratios were modified (Figure 2b). The modification proposed by De Risi et al. [48] significantly reduced

the CoV values for tests performed on hollow bricks with respect to the original formulation by Panagiotakos and Fardis [38]. The accuracy of the provided model is also proved by the observation that the resulting backbone curve mean relative error was lower than 3% for all required parameters.

In the De Risi et al. [48] model the first branch corresponds to the elastic behavior up to cracking, and is characterized by the initial un-cracked stiffness (K_0), assumed equal to 2.8 times the Mainstone's stiffness (K_{MS}) [31]. The K_{MS} is obtained adopting in Equation (7) the equivalent strut width defined as follows:

$$b_w = 0.175(\lambda_h h_w)^{-0.4} d_w \quad (8)$$

where λ_h is defined in Equation (6).

The infill cracking strength is $F_{cr} = 0.7 \cdot F_{peak}$, where F_{peak} is equal to the lateral cracking strength of the Panagiotakos and Fardis [38] model:

$$F_{peak} = \tau_{m0} t_w l_w \quad (9)$$

The second branch continues up to the peak strength (F_{peak}), and the secant-to-peak stiffness corresponds to $0.8 \cdot K_{MS}$. The third branch is a degrading branch up to zero residual lateral strength defined by degrading slope (K_{deg}) assumed equal to $K_{deg} = -0.1 \cdot K_{MS}$.

More recently, Huang et al. [49] (Figure 2c) proposed the adoption of a backbone curve calibrated on experimental results. Similar to De Risi et al. [48], the authors collected a database of 264 tests performed on masonry-infilled frames. Based on the analysis of the database, the authors developed an empirical model for estimating the backbone curve parameters for the equivalent diagonal strut. The main difference between the model by De Risi et al. [48] and Huang et al. [49] is the way the backbone curve is calibrated. In particular, De Risi et al. [48] started from the proposal by Panagiotakos and Fardis [38] and modified existing semi-empirical formulations in order to reduce the scatter with respect to their database. Instead, Huang et al. [49] developed empirical equations to relate different backbone parameters to several geometric and material properties of the infilled frame using multivariate regression analysis. In this work, only median values of the backbone parameters were adopted.

Differently from the work by Bertoldi et al. [37] and De Risi et al. [48], which provide the force-displacement curve for the infill strut, Huang et al. [49] provides formulations in terms of axial force/axial deformation (N, Δ_a) for the infill strut. The first branch of the lateral response backbone is defined by the elastic stiffness up to cracking ($K_{a,0}$) which can be calculated as:

$$K_{a,0} = 0.0143 E_w^{0.618} t_w^{0.694} \left(\frac{h_w}{l_w} \right)^{-1.096} \quad (10)$$

and the cracking strength (N_{cr}) that is assumed as a ratio of the peak strength N_{peak} :

$$N_{cr} = 0.72 N_{peak} \quad (11)$$

where:

$$N_{peak} = 0.003766 \cdot \sigma_{m0}^{0.196} t_w^{0.867} l_w^{0.792} \quad (12)$$

The second branch corresponds to the post-cracking behavior, and is defined once that F_{peak} and Δ_{peak} are defined. The Δ_{peak} can be calculated as follows:

$$\Delta_{a,peak} = 0.0154 E_w^{-0.197} \left(\frac{h_w}{l_w} \right)^{0.978} d_w \quad (13)$$

The third branch describes the post-peak behavior and is characterized by a degrading slope (K_{deg}) up to residual strength:

$$K_{a,deg} = -1.278 \sigma_{m0}^{-0.357} t_w^{-0.517} K_0 \quad (14)$$

Finally, the residual strength is defined as:

$$N_{res} = 0.4N_{peak} \quad (15)$$

The constitutive models reported above describe the behavior of solid infills. When openings are present to accommodate windows or doors, experimental results still highlighted that the presence of infills enhances the performance of RC frames, but with a reduced effect with respect to a solid infill wall. Generally, the presence of openings leads to a reduction in stiffness, strength, and energy dissipation and also modifies the crack pattern depending on the position and size of openings [51].

To simulate the presence of openings, the most common approach consists of indirectly reduce the strength and the stiffness of the infill panel depending on the opening size, reducing the width of the diagonal strut by adopting an approximate reduction factor [39,46,52–55]. However, some authors evidenced that both the location [52] and the shape ratio [54] of openings influence the frame global performance and, in some cases, it can lead to the development of brittle shear failure (e.g., in the case of partially-infilled frame).

For example, the formulation proposed by Decanini et al. [54] accounts for both the openings percentage and shape ratio:

$$\rho = 0.55 \exp(-0.035\alpha_a) + 0.44 \exp(-0.025\alpha_l) \quad (16)$$

where:

$$\alpha_a = \frac{l_0 h_0}{l_w h_w} \quad (17)$$

where l_0 , h_0 , l_w , h_w are indicated in Figures 2 and 3.

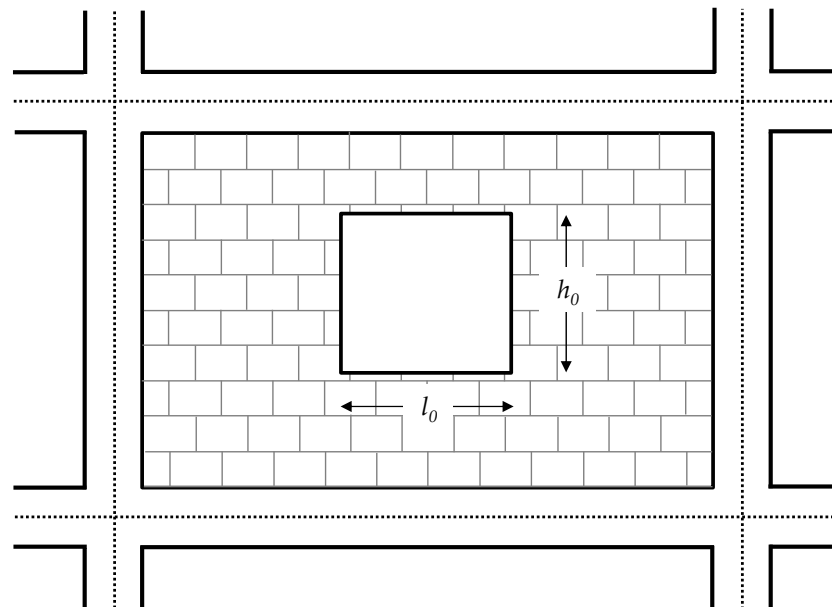


Figure 3. Opening notation adopted in this study.

2.3.2. Single-Strut Cyclic Law

When adopting the equivalent strut approach to perform nonlinear time-history analyses, it is of crucial importance to select the more appropriate cyclic law to realistically simulate the hysteretic behavior of the masonry infills. The adopted hysteretic law should be able to capture the strength and stiffness deterioration, the loading and unloading cycles, and the residual strength with sufficient accuracy. Since the cyclic behavior of masonry infills is very difficult to capture, several proposals were made to describe the actual behavior of infill panels. The first proposal of a hysteretic model was made by

Klingner and Bertero [56] based on results from a single dynamic test. The model was later modified by Cavalieri et al. [57,58] to enhance the description of loading and unloading branches, and to include the effect of pinched behavior. In this case, the model only requires the definition of three parameters related to pinching and degradation behaviors. Later, Panagiotakos and Fardis [38] extended the model by Tassios [59] and proposed a three-parameters hysteretic model. Crisafulli [24,60] developed a more sophisticated cyclic model in order to simulate different failure mechanisms. However, the latter model is of difficult implementation since requiring a large number of parameters to calibrate. Lately, several authors focused on the calibration of existing hysteretic models available in different software environments to describe the cyclic behavior of infills. For instance, the Hysteretic material and Pinching4 material [61] were adopted to simulate the only-compression strut axial behavior in OpenSees [19,62]. However, Noh et al. [19] compared two different modeling strategies to reproduce the hysteretic behavior of infill struts and found that the Pinching4 material is the most suitable to reproduce actual response under cyclic loadings of masonry infills.

The pinching4 material is often adopted due to its capability of modeling nonlinearity and degradation of stiffness and strength under cyclic loading. The material model requires the definition of 15 parameters controlling strength, unloading, and reloading stiffness degradation, as a function of ductility and/or energy demand, and 6 parameters controlling pinching behavior. However, due to the significant effort required for the calibration of the full suite of parameters, it is common procedure to relate various degradation modes only to the displacement or energy history in order to reduce the effort required during the calibration procedure. The parameters required to define this material hysteric behavior can be obtained following different authors and international code recommendations. For instance, Lima et al. [63] calibrated Pinching4 parameters by comparing numerical analyses and experimental tests on masonry walls performed by Koutromanos et al. [64]. Kumar et al. [65], based on the results of experimental tests [66], proposed two different sets of hysteretic parameters for Pinching4 material depending on the rigidity of the panel (“weak” or “strong” infills). While previous studies calibrated Pinching4 material based on a very limited number of tests, Huang et al. [49] performed a visual calibration for a large database composed of 113 experimental tests. However, the authors did not perform a regression analysis to relate pinching and cyclic degradation parameters to infill properties, only providing the appropriate range of variation for parameter values.

3. Research Methodology

Numerous modeling approaches were proposed over the last decades to simulate the lateral response of masonry-infilled RC frames. Depending on the modeling strategy and the response envelope adopted, the results in terms of building response may significantly vary. This leads to significant uncertainty as to which is the most appropriate analytical models for the assessment of seismic performances of masonry-infilled frames, with non-negligible implications, especially when dealing with large-scale simulation purposes.

Without expecting to be exhaustive, this study analyzes the effect of alternative constitutive relationships on the global response of buildings in order to quantify the differences in terms of engineering demand parameters. Among the proposed modeling approaches, the single-strut allows accounting for the contribution of infill panels in terms of global stiffness and strength and displacement capacity still preserving a good level of accuracy [67]. As a consequence, it can be adopted to assess the influence of adopted constitutive relationship on the seismic response of building in terms of engineering demand parameters such as interstory drift ratios and peak floor accelerations for different intensities of ground motion demand. The effect of different strut constitutive models available in the literature is investigated adopting three alternative constitutive laws described in detail in Section 2. In particular, (1) the differences in terms of backbone curve for a single infill panel are evidenced both at the local and the global level adopting a pushover analysis. By performing nonlinear time history analyses employing a set of 42

far-field ground motion records, the effect of the constitutive envelope on the attainment of a given level of damage is quantified at the global level (2) by generating damage state fragility functions, and (3) by evidencing the effect of the constitutive model on the amounting and distribution of engineering demand parameters such as interstory drift ratios and peak floor accelerations.

4. Numerical Model for the Case-Study Building

In order to investigate the influence of the constitutive law of the equivalent strut on the seismic performance of a masonry-infilled RC frame, a four-story building located in L'Aquila designed according to obsolete seismic standards was studied. The building was constructed at the beginning of the 1980s and suffered damage due to the 2009 L'Aquila earthquake.

The building structural system consists of three planar RC frames oriented in the longitudinal direction, connected each other by flat beams in the transverse direction except for the transverse perimeter frame where deep beams are adopted. The building is regular both in plan and elevation and has an in-plane shape that can be inscribed in a rectangle of 17 m × 10 m. The interstory height is equal to 3.25 m except for the roof story, for which it is equal to 2.65 m. According to the design and construction practice in force at the time of construction, the geometry and reinforcing details of each structural member are the same for all frames in the same direction and for each story. Exterior frames in both directions are infilled with hollow clay bricks with thickness $t_w = 30$ cm (strong infill). The openings vary between each span and story. For further details refer to Gaetani d'Aragona et al. [68].

In this study, a three-dimensional finite element model is developed in OpenSees (Version 3.2.0, University of California, Berkeley, CA, USA) with the aim of evaluating the performances of RC masonry-infilled frames under earthquake loadings. Due to the reduced in plan dimensions and the presence of an inclined reinforced concrete roof, the upper story is modeled as an equivalent load mass, assuming it behaves as a rigid body.

Figure 4a shows the 3D perspective view of the reference building, while Figure 4b shows a schematic representation of the three-dimensional finite element model.

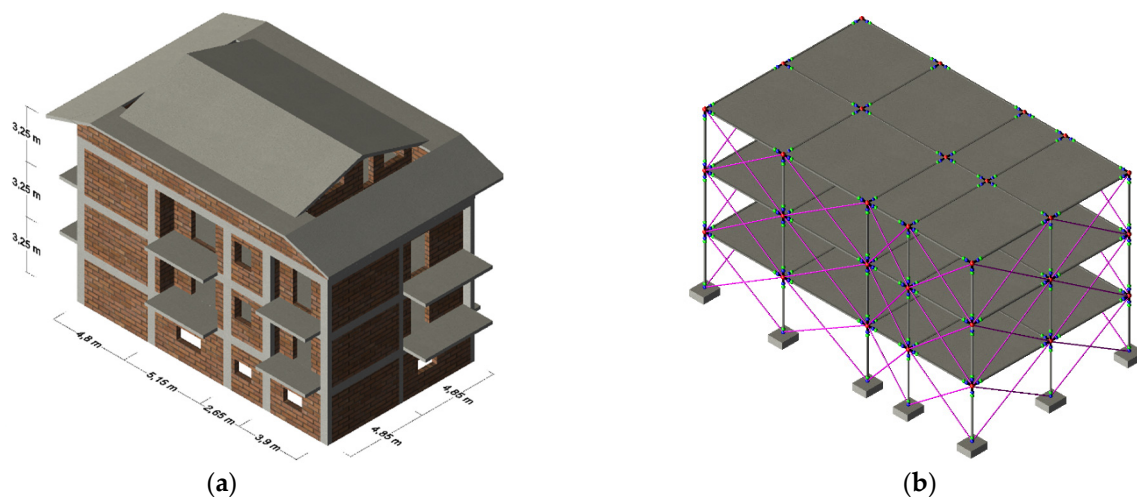


Figure 4. Case-study building (a) solid view and (b) finite element model (adapted from Gaetani d'Aragona et al. [68,69]).

When subjected to earthquake loadings, existing infilled RC buildings designed according to obsolete seismic code provisions may exhibit brittle mechanisms due to the non-ductile behavior of RC members. For this reason, the finite element model should properly account for the effects that may develop in poorly detailed frame members (e.g., widely spaced stirrups, 90°-hooks, lacking stirrups in the panel joint region) that are characterized by non-ductile behavior. Along with mechanical and geometrical nonlinearities, the possi-

ble brittle failure of beam-column joints, of RC columns, the bar-slip at members end need to be explicitly simulated via the finite element model (Gaetani d’Aragona et al. [68,69]).

In this study, a lumped plasticity approach already proposed in Gaetani d’Aragona et al. [68,69] is adopted to develop the numerical model of the case-study building (Figure 5). In particular, beams and columns are modeled adopting mono-dimensional beam-column elastic elements while the inelastic behavior is concentrated in zero-length rotational springs at either end. The stiffness of single in series elements composing the sub-assembly is calibrated to reproduce the actual stiffness of sub-assembly. The inelastic behavior of beam/column rotational springs is conveniently characterized by a multilinear moment–rotation backbone curve with cracking and yielding as initial characteristic points. Three possible failure modes (flexure, flexure-shear, or pure shear failure) are considered for RC columns accounting for possible brittle failure of non-conforming members. The hysteretic behavior of the moment-rotation springs is simulated adopting the Pinching4 material with the hysteretic rules proposed for older reinforced concrete members. P-Delta effects are considered. The longitudinal bar-slip effect in columns, beams, and beam-column joints is modeled by adding zero-length inelastic springs at either end of the beams and columns in order to account for a possible increase in lateral deflection due to the slippage effect. No hysteretic degradation is assumed for these elements. The non-linear shear deformation of the panel joint region is simulated by adopting a “scissor” model. Rigid offset depending on the dimension of converging members is included to account for the finite dimension of the panel joint. The pinched hysteretic behavior for beam-column joints is simulated adopting the Pinching4 material. Finally, the presence of RC one-way slabs is simulated via an elastic shell element connecting the main nodes of the frame at the same height. A 5% Rayleigh damping is assigned to the first and the third modes, and damping coefficients are applied to mass and committed stiffness matrixes.

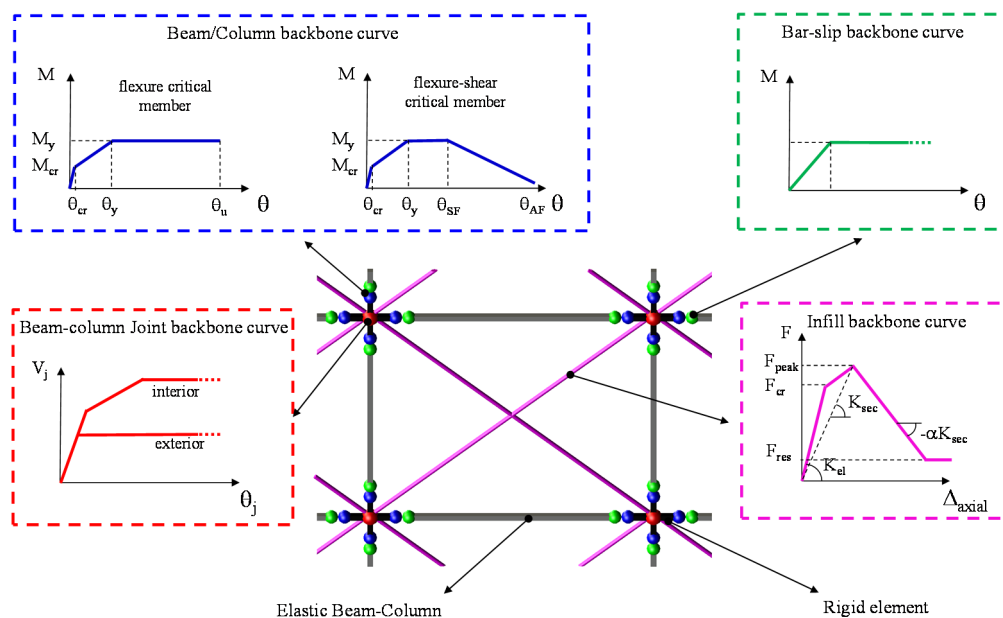


Figure 5. Numerical modeling for frame and infill elements (for further details refer to Gaetani d’Aragona et al. [68,69]).

The characterization of structural members backbone curve is defined based on member geometries, reinforcement details, and material properties available in structural drawing and performed material tests. For further details about RC members’ material properties, backbone curves and hysteretic parameters adopted for the finite element model refer to Gaetani d’Aragona et al. [68,69].

Regarding the presence of masonry infills, the equivalent strut modeling approach is adopted. For each panel, the pin-jointed strut is simulated by employing a concentric

nonlinear truss element in which the axial stress-deformation backbone curve and the hysteretic behavior is simulated adopting the Pinching4 material [61] adopting the parameters proposed by Lima et al. [63]. Very small values are assumed for the definition of the tensile part of the backbone curve in order to obtain only-compression behavior. The three constitutive laws describing the behavior of infill panels reported in Section 2.3.1 are employed. Pinching and damage parameters defining the cycling degradation for infill masonry proposed in Lima et al. [63] are adopted.

The applicability of the adopted models requires the definition of the mechanical properties mentioned in Equations (1)–(15). In particular, shear cracking strength (τ_{m0}), Young's modulus (E_w), and shear modulus (G_w) of masonry panel are required to define the backbone curve according to De Risi et al. [48]. Similarly, the model by Huang et al. [49] only requires the strength of the masonry prism (σ_{m0}) and Young's modulus (E_w), while more mechanical parameters are needed for the implementation of the model proposed by Bertoldi et al. [37].

According to the original design drawings available for the case-study building, the infill walls are made of hollow clay bricks with a thickness $t_w = 30$ cm. With reference to the work by Hak et al. [70], the mechanical properties for strong infill masonry are adopted ($E_w = 3240$ MPa). The shear modulus of the masonry (G_w) is taken as 0.40 times the Young's modulus of the masonry (E_w) according to FEMA 356 [71]. The value of the shear strength (τ_{m0}) is obtained via linear interpolation between the boundary values proposed in Circolare 7 [72] as a function of Young's modulus. The masonry compressive strength (σ_{m0}) is calculated as $\sigma_{m0} = (\tau_{m0}/0.285)^2$ and the bed joints sliding strength τ_0 is obtained from the empirical relationship $\tau_0 = 2/3 \tau_{m0}$ [73]. The values of mechanical properties adopted in his study are reported in Table 1.

Table 1. Mechanical properties of masonry infills.

t_w (mm)	E_w (MPa)	G_w (MPa)	τ_{m0} (MPa)	τ_0 (MPa)	σ_{m0} (MPa)
300	3240	1296	0.34	0.23	1.53

t_w : thickness; E_w : Young's modulus; G_w : shear modulus; τ_{m0} : shear strength; τ_0 : shear sliding strength of bed joints; σ_{m0} : masonry compressive strength.

To account for the presence of openings in the infill panels, the equivalent strut width is reduced by a factor that depends on the percentage and the shape of the opening in the panel according to Decanini et al. [54]. The opening percentage varies at different stories and for each span. In particular, in the X direction, the opening percentages for different infill panels varies approximately in the range 0–34% at the different stories, while in the Y direction it varies in the range 0–12% in the first story and 0–30% for other stories.

5. Influence of Modeling Assumptions

In this section, a first comparison between the different constitutive models reported in Section 2.3.1 is performed at the local level, for a single infill panel, and at the global level, to quantify the dependence of the lateral building response on the constitutive law. Firstly, the comparison is performed for a single panel in order to quantify the difference between backbone curves for given geometrical and mechanical properties.

With reference to a solid infill panel (i.e., without openings) the three formulations indicated in Section 2.3.1 lead to significantly different constitutive models for the equivalent strut both in terms of strength and stiffness. Figure 6 depicts the comparison for the panel with $H = 2.80$ m and $L = 4.80$ m in Figure 4a. In terms of stiffness, for Bertoldi et al. [37] (BR) and De Risi et al. [48] (DR) the initial un-cracked stiffness K_0 indirectly depends on the same geometric (l_w, h_w, I_c) and mechanical (E_w, E_c) parameters of both the masonry infill and the surrounding RC frame, while for Huang et al. [49] (HG) it only depends on the masonry infill properties (l_w, h_w, E_w). For the selected infill panel, the initial stiffness for three backbone curves are $K_{0,BR} = 8.01 \times 10^5$ kN/m, $K_{0,DR} = 2.67 \times 10^5$ kN/m,

$K_{0,HG} = 1.16 \times 10^5$ kN/m. Taking the stiffer lateral response predicted by BR as a reference value, the initial stiffness predicted by DR is 33% and the one predicted by HG is 14% the value predicted by BR. This difference at the local level significantly influences the initial response of the building, and the elastic forces transmitted to the building at the initial uncracked stage, as can be evidenced by the fundamental period of the building. With reference to the peak force F_{peak} (Table 2), the model by BR explicitly accounts for the different possible failure modes for the infill and leads to the lower value of $F_{peak} = 208.0$ kN (corresponding to diagonal tension) with respect to other authors. In this case, DR and HG predict similar peak forces that are about $F_{peak} = 347.0$ kN and $F_{peak} = 339.0$ kN, respectively, which are about 166% and 162% the value predicted by BR. Similar considerations can be carried out for the value of cracking force. In terms of residual force (F_{res}), BR leads to $F_{res} = 72.8$ kN and HG to about twice (186%) this value, while no residual force is considered by DR.

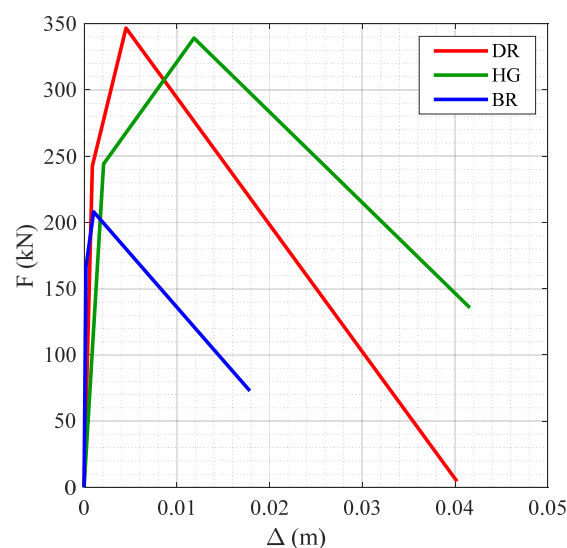


Figure 6. Lateral force-displacement equivalent strut backbone curves for a solid infill panel adopting DR, HG, and BR.

Table 2. Backbone curve points for the reference infill panel.

Backbone Points	BR	DR	HG
Δ_{cr} (m)	2.07×10^{-4}	9.04×10^{-4}	2.10×10^{-3}
Δ_{peak} (m)	1.04×10^{-3}	4.52×10^{-3}	1.19×10^{-2}
Δ_{ult} (m)	1.80×10^{-2}	4.02×10^{-2}	4.16×10^{-2}
F_{cr} (kN)	166.4	242.7	244.2
F_{peak} (kN)	208.0	347.0	339.0
F_{res} (kN)	72.8	0.0	135.6

Another remarkable difference between the proposed backbone curves is in terms of lateral displacement values (Table 2). BR is the most conservative always predicting lower values of lateral displacement, and a significant difference exists also between DR and HG. Regarding the displacement at cracking (Δ_{cr}) similar considerations can be carried out to those for the initial stiffness. For the peak displacement (Δ_{peak}), taking as a reference the value predicted by BR, DR and HG predict significantly larger values, equal to 4.34 and 11.44 times the value predicted by BR, respectively. Finally, the ultimate displacement (Δ_{res}) predicted by DR and HG is 2.23 and 2.31 times the value by BR, respectively.

The choice of constitutive law has a significant effect on the global response of masonry-infilled RC frames. This effect depends on the relative contribution to lateral strength of the infill panels with respect to the RC frame, and reduces as the opening percentage increases, up to possibly erase the infill contribution. The contribution of the infills on the

lateral response of RC frames can be clearly quantified by performing a static pushover analysis. Adopting first mode-proportional loads, the pushover analysis is performed both along the longitudinal and transverse direction in order to visualize the lateral response under increasing loads. In particular, Figure 7a,c represents the pushover response for the actual infill opening configuration performed in the longitudinal (transversal) direction, considering the three constitutive laws reported in Section 2.3.1, and the finite element model described in Section 4. For comparison purposes, the response of the bare frame is also reported.

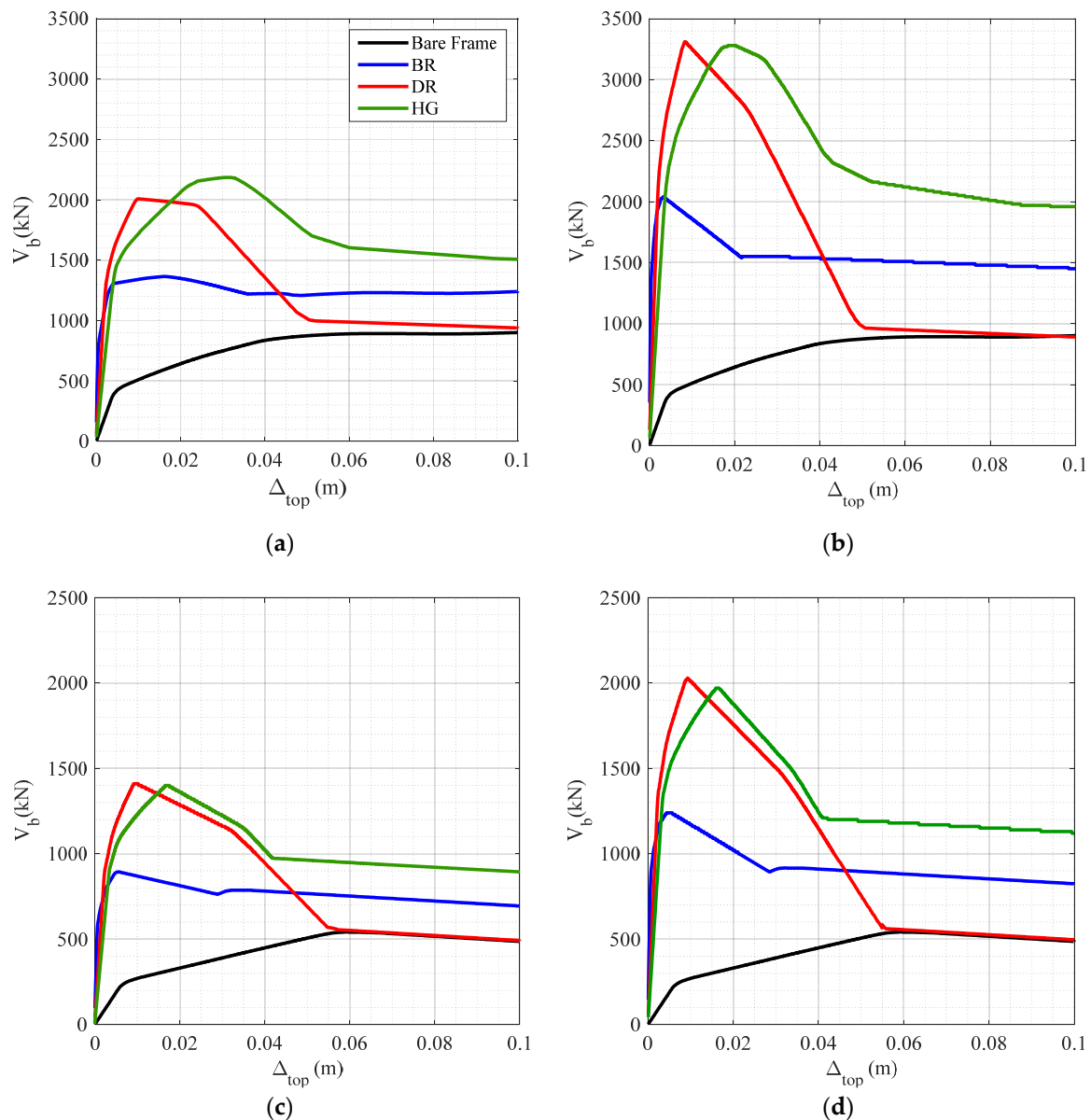


Figure 7. Pushover curves in the longitudinal (a,b) and the transverse (c,d) direction for (a,c) the actual opening configuration and (b,d) simulating no openings, obtained adopting DR, HG, and BR constitutive laws.

Note that for the case-study building, no brittle failure of RC members is detected when analyzing the building response in the longitudinal direction, while shear failure after rebar yielding was detected in the transverse direction. For this reason, in the longitudinal direction, the pushover curve for bare frame shows a horizontal branch after peak base shear, while in the transverse direction a degrading slope is displayed. In order to quantify the maximum contribution to lateral strength of infill as a function of the selected

constitutive law, the pushover response simulating that no openings are present in the infill panels is also reported for the longitudinal direction in Figure 7b and the transverse direction in Figure 7d. If no openings are present in the masonry panels, infills provide the maximum contribution to lateral strength. By comparing the different infill backbone curves in terms of maximum strength: BR, DR, and HG show a maximum base shear (V_b) with respect to the bare frame that is 227%, 368% and 365% greater, respectively. If the actual infill configuration is considered, and the equivalent strut width is modified according to Equations (16) and (17), the contribution of infills to lateral strength reduces to 152%, 223%, and 243% for BR, DR, and HG, respectively. Due to the presence of opening, the maximum base shear reduces by about 33% for BR and HG, while of 39% for DR. The relative difference, in terms of V_b , between the different backbone curves remains almost unaltered between the no-opening and actual opening configurations, suggesting that the distribution of openings is sufficiently regular to avoid the development of soft-story mechanism or changing the collapse mechanism of the building with respect to uniform distribution of openings (i.e., no openings). In the transverse direction, the maximum contribution to base shear (i.e., no openings) is about the same that was evidenced in the longitudinal direction, being equal to 229%, 366%, and 375% for BR, DR, and HG, respectively. When the actual opening configuration is considered, this contribution to lateral resistance drops to 165%, 259%, and 261%, which corresponds to a reduction of maximum base shear of 27%, 29%, and 30% for BR, DR, and HG, respectively.

The adoption of different constitutive law significantly influences the initial elastic stiffness of the building. While for the bare frame analyzed in the longitudinal direction, the fundamental vibration period is $T_{1X,bare} = 0.68$ s, for the different constitutive laws, and actual opening configuration, the vibration periods are $T_{1X,BR} = 0.11$ s, $T_{1X,DR} = 0.17$ s and $T_{1X,HG} = 0.23$ s. The differences in terms of vibration period may significantly affect the seismic demand at the uncracked stage of the structure, and the evolution of damage also in the nonlinear stage. In the transverse direction, due to the reduced in plan extension with respect to the longitudinal one and to the lower number of spans and infill panels, the structure results more deformable, with $T_{1Y,bare} = 0.83$ s, for the different constitutive laws, and actual opening configuration, the vibration periods are $T_{1Y,BR} = 0.13$ s, $T_{1Y,DR} = 0.20$ s and $T_{1Y,HG} = 0.24$ s.

6. Results of NRHAs

This section presents the results obtained via a nonlinear response history analysis (NRHA) performed on the three-dimensional finite element model (FEM) described in Section 4. The NRHA is performed adopting 42 earthquake records from the far field set reported in FEMA-P695 [74]. Analyses are performed for different values of the seismic action, by scaling the earthquake intensity, expressed in terms of peak ground acceleration (PGA), between 0.05 g and 1.5 g with a step of 0.05 g. The building response is analyzed separately in the longitudinal and the transverse direction.

The first comparison is performed in terms of damage state fragility function, which defines the probability of exceeding a damage state as a function of a ground motion intensity (IM):

$$P(DS \geq ds_i | IM) \quad (18)$$

The PGA was selected as IM since it is independent of the elastic characteristics of the buildings and allows a comparison between results obtained from structures with different initial elastic characteristics. Under the hypothesis that the IM values of ground motions causing the attainment of a DS are lognormally distributed, the functional form for the cumulative distribution function is:

$$P(DS \geq ds_i | PGA) = \Phi\left(\frac{\ln(PGA/\theta)}{\beta}\right) \quad (19)$$

where $\Phi()$ is the standard normal cumulative distribution function, θ is the median of the fragility function and β is the logarithmic standard deviation. The parameters θ and β are

estimated by adopting the maximum likelihood estimation (MLE) technique [75] to fit the results, which searches for the parameter values that are most likely to have produced the data. By assuming a binomial distribution to describe the probability that z_j ground motion records with a given PGA, over n_j total ground motions, caused the attainment of damage state ds_i , the likelihood function considering m levels of the seismic action is expressed as the product of binomial probabilities at each PGA level:

$$Likelihood = \prod_{j=1}^m \binom{n_j}{z_j} P(DS \geq ds_i | PGA)^{z_j} [1 - P(DS \geq ds_i | PGA)]^{n_j - z_j} \quad (20)$$

where \prod denotes the product over all ground motion levels. The MLE technique allows the calculation of the fragility function parameters by maximizing the Likelihood function (Equation (20)). Further, this procedure provides reliable results also in case of truncated IDA (i.e., when the analysis is performed up to a given value of the IM) [75]. Note that neither variability in material properties nor in the geometrical features are considered in this study, and the dispersion in results for a structural model with a given constitutive law only depends on the record-to-record variability.

Five damage states (DSs) are defined compatibly with the EMS-98 scale [76] and expressed in terms of interstory drift ratio (Table 3). Starting from the simplified procedure proposed in Gaetani d’Aragona et al. [20], which allows to perform a simplified Pushover analysis by adopting a closed-form procedure, the attainment of EMS98-like DSs [77] are identified during the generation of the pushover curve and transformed in the corresponding interstory drift ratios.

Table 3. Damage state thresholds in terms of interstory drift ratios defined according to EMS-98 scale.

DS ₁	DS ₂	DS ₃	DS ₄	DS ₅
0.03%	0.32%	1.03%	3.30%	3.70%
Concrete cracking/Onset infill cracking	Rebar yielding/Moderate infill cracking	Rebar buckling/cover spalling/First column shear failure/Extensive infill cracking	First column axial failure/ultimate capacity	All story columns exhibit axial failure/ultimate capacity

The damage states are defined depending on the attainment of local phenomena exhibiting by infill panels (i.e., extension of cracking) or the RC frame (i.e., rebar yielding, buckling, concrete spalling, shear, axial failure, or attainment of maximum chord rotation for ductile members). The displacement corresponding to different DSs slightly varies depending on the constitutive law adopted for infills and on the analysis direction. For simplicity purposes, a mean value is assumed for each DS between different constitutive laws and directions.

The adoption of different constitutive laws for the equivalent strut may significantly affect the PGA value at which the damage state DS_i is attained. To quantify this effect, the Damage State fragility functions expressed in terms of PGA are reported in Figure 8 for the three constitutive laws adopted in this study (BR, DR, HG) by separating the results in the longitudinal (Figure 8a) and the transverse (Figure 8b) directions. The medians (θ) and the logarithmic standard deviations (β) are also reported for the longitudinal (Table 4) and the transverse (Table 5) direction.

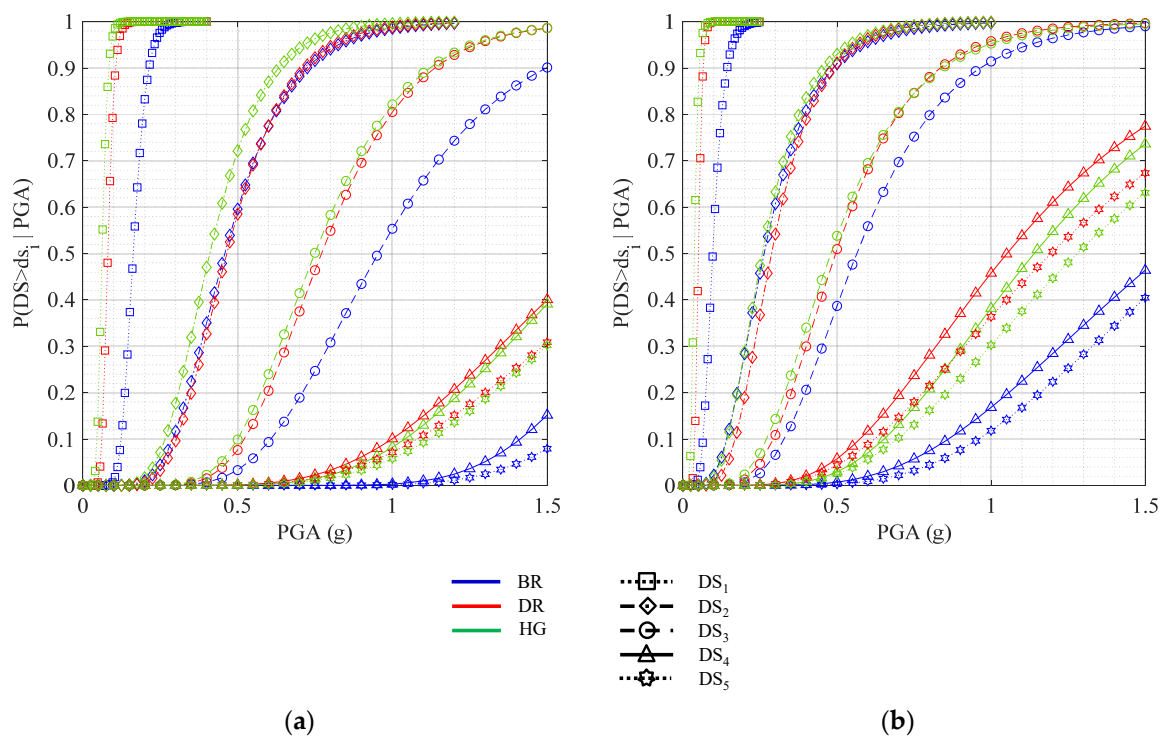


Figure 8. Fragility curves corresponding to the attainment of EMS-98 damage states in the (a) longitudinal and (b) transverse direction adopting DR, HG, and BR constitutive laws.

Table 4. Lognormal fragility curve parameters in the longitudinal direction.

		Longitudinal Direction									
		DS ₁		DS ₂		DS ₃		DS ₄		DS ₅	
Backbone model	θ	β	θ	β	θ	β	θ	β	θ	β	
BR	0.16	0.21	0.46	0.36	0.95	0.35	1.91	0.24	2.15	0.25	
DR	0.08	0.21	0.47	0.34	0.77	0.30	1.66	0.40	1.85	0.42	
HG	0.06	0.24	0.41	0.34	0.75	0.31	1.66	0.36	1.83	0.38	

Table 5. Lognormal fragility curve parameters in the transverse direction.

		Transverse Direction									
		DS ₁		DS ₂		DS ₃		DS ₄		DS ₅	
Backbone model	θ	β	θ	β	θ	β	θ	β	θ	β	
BR	0.10	0.31	0.26	0.48	0.56	0.42	1.56	0.47	1.66	0.43	
DR	0.05	0.21	0.29	0.41	0.50	0.41	1.05	0.47	1.19	0.51	
HG	0.04	0.28	0.26	0.45	0.48	0.44	1.14	0.43	1.28	0.48	

Observing damage state fragility curves in Figure 8, it can be noted that they reflect the variation in lateral stiffness of the system, which is related to the adopted infill backbone curve. In fact, according to observations in Section 5, the BR backbone curve leads to the most rigid behavior, while for DR and HG the initial stiffness reduces. This observation is valid for both directions. For DS₁, where first nonlinearities occur in the structure, the seismic response is expected to be close to that in the linear range. In fact, DS₁ firstly occurs for HG, which corresponds to the more deformable system, followed by DR and BR. This trend is confirmed also for higher damage states despite the scatter between fragility curves for the three backbone curves is not constant. With reference to the longitudinal direction,

by adopting BR as a reference response, the difference in terms of median PGA that leads to DS_i for DR backbone curve is -50% for DS_1 , while drops to -1% and -20% for DS_2 and DS_3 , respectively. For both DS_4 and DS_5 the difference again grows to about -13% . For the HG backbone curve, the difference with respect to BR is about -60% for DS_1 , while for DS_2 drops to about -10% and from DS_3 to DS_5 is about -15% . Similar trends are shown in the transverse direction, where the scatter with respect to BR backbone curve is comparable for both DR and HG, except that for DS_4 and DS_5 where the scatter is between 1.5 to 2.5 times that in the longitudinal direction. It is also worth noting that in both the directions, for DS_1 to DS_3 , the DS_i is attained for lower PGA values for HG with respect to DR, while for DS_4 and DS_5 , the trend is inverted, since the DS_i first occurs for DR. This effect is more clear when observing the transverse direction (Figure 8b).

In the transverse direction, the attainment of different DSs generally corresponds to lower PGA values with respect to the longitudinal direction. This is due to the reduced lateral stiffness of the system in the transverse direction when compared to the longitudinal one, confirmed by higher values of the fundamental period of vibration (see Section 5), which leads to higher lateral deformations for the same PGA value. In particular, the scatter between the two orthogonal directions is around 40% for DS_1 to DS_3 , and reduces as the damage increases with a minimum value for DS_4 and DS_5 (18–36%). Finally, it can be noted that higher dispersion occurs in the transverse direction for all considered DSs. The influence of the constitutive law on the structural behavior can be also evidenced by means of other response quantities. One way to express the seismic performances of a building is the use of engineering demand parameters (EDPs) such as interstory drift ratios (IDRs) and peak floor accelerations (PFAs). The EDPs are response quantities of particular interest when the damage to both structural and nonstructural components need to be estimated and are at the base of the PBEE framework [78] procedures that allow the estimation of repair costs.

Figure 9 shows the IDR profiles in the longitudinal direction for PGA values corresponding to median PGAs for damage states from DS_1 to DS_4 , that are 0.1 g–0.4 g–0.6 g–1.2 g (Table 4), respectively. The IDR profiles are obtained as median value between the 42 ground motion responses. For the lower value of the seismic intensity (Figure 9a), for which it is expected that the structure almost behaves elastically, a high scatter between the IDRs between the three models is attained. DR and HG predict IDRs equal to 2.7 and 5.9 times that predicted by BR, respectively. Further, the IDR is very similar for the first and the second story, but for DR and HG the maximum IDR occurs at the second story and in the first story for DR. As the intensity increases, the difference in prediction between different models reduces and the maximum IDR concentrates in the first story. For $PGA = 0.4$ g (Figure 9b) HG still predicts larger IDRs with respect to BR, while DR leads to lower IDRs. In particular, DR leads to IDR_{max} which is 4% lower with respect to BR, and HG to 32% higher. For $PGA = 0.6$ g (Figure 9c), the scatter with respect to BR is 16% and 28% for DR and HG, respectively. For $PGA = 1.2$ g (Figure 9d) and higher earthquake intensities, the IDRs for DR and HG are close to each other and predict 56% and 50% larger IDRs with respect to BR, respectively. Note that for PGA varying from 1.0 g to 1.5 g, DR always predicts larger IDRs with respect to HG, while the trend is inverted for intensities lower than 1.0 g.

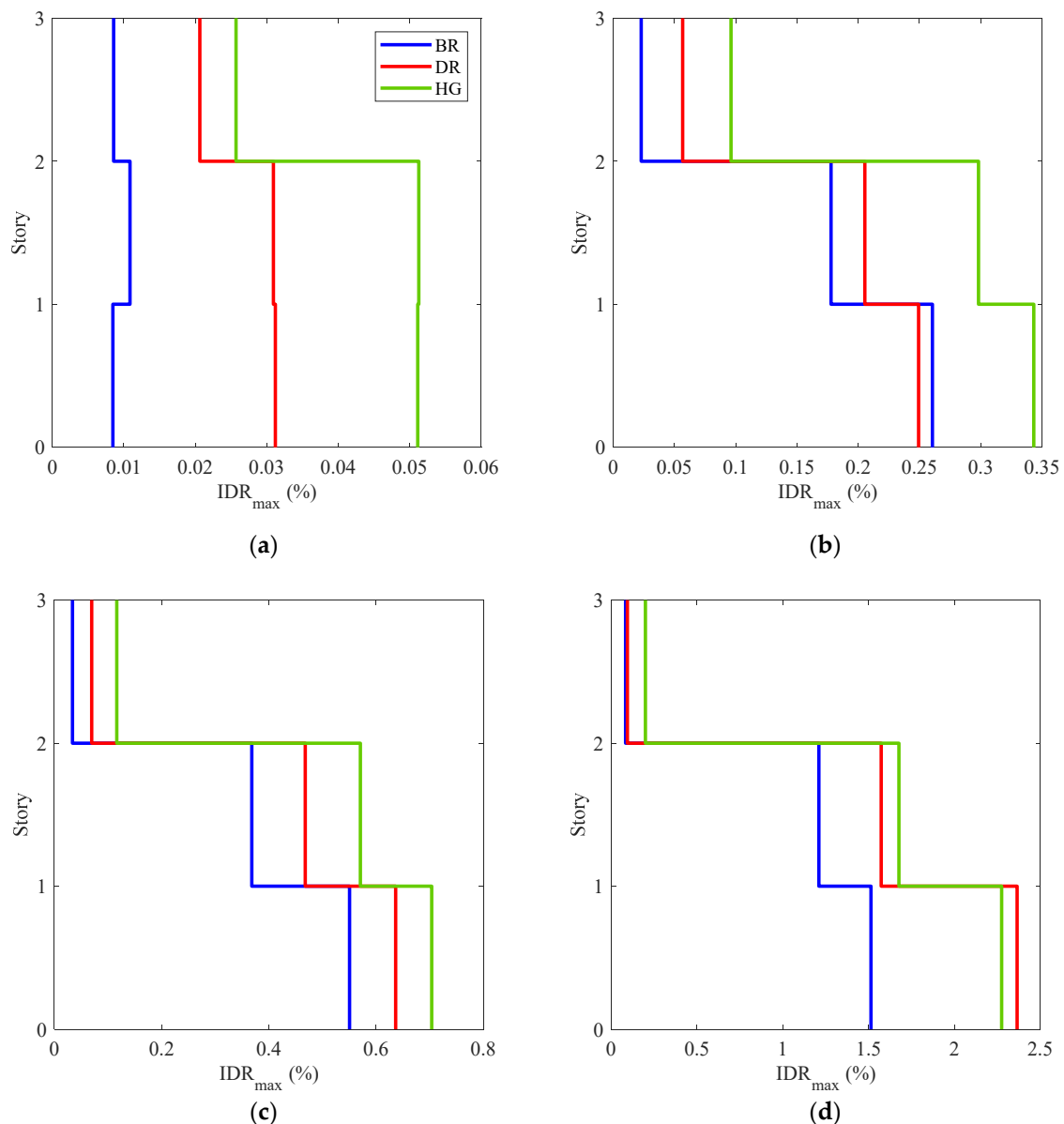


Figure 9. Interstory drift profiles in the longitudinal direction for PGA corresponding to (a) 0.1 g, (b) 0.4 g, (c) 0.6 g, (d) 1.2 g.

In the transverse direction (figure not shown here for brevity reasons), the analyses led to similar results to the longitudinal direction. However, some major difference arises. In particular, for $PGA = 0.1$ g the different backbone curves still lead to a high scatter between the three results, but in this case, the maximum IDR always occurs in the first story. While in the longitudinal direction, where the drift demand is well distributed along the height, in the transverse direction, as the intensity of ground motion increases, the damage concentrates in the first story, while upper stories are relatively less damaged. For instance, for $PGA = 0.4$ g the IDR at the second story is 20% to that in the first one. This trend is confirmed for higher intensities, where the IDR at the second story is generally comprised between 20% and 30%. This may be ascribable to the higher deformability of the structure in the transverse direction with respect to the longitudinal one, which leads to IDRs that almost twice those in the transverse direction for the same PGA value.

In terms of peak floor accelerations, the median profiles along the height are reported in Figure 10 for PGA equal to 0.1 g–0.4 g–0.6 g–1.2 g. It is interesting to note that for $PGA = 0.1$ (Figure 10a), when the structure is almost elastic, the PFA increases almost linearly with the height. For $PGA = 0.4$ g, which about corresponds to DS_2 , lower values

along the height with respect to those expected during elastic behavior are predicted. In particular, for BR the reduction of PFAs along the height indicates a higher level of damage with respect to DR and HG. As the damage spreads through the structure, the ratio PFA/PGA decreases in upper stories. This effect is particularly evident for $PGA = 1.2\text{ g}$ where the PFA decreases along the height.

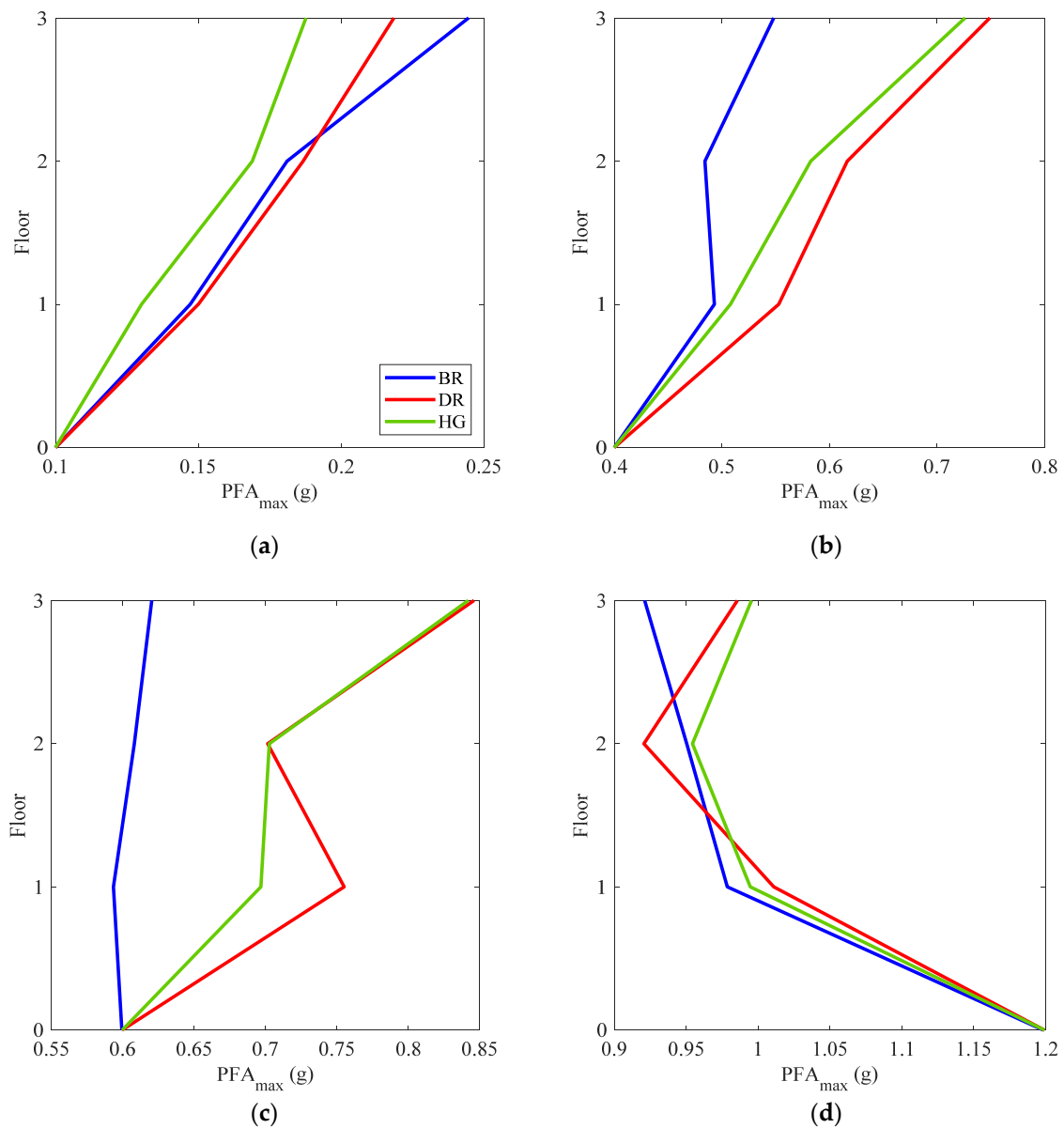


Figure 10. PFA profiles in the longitudinal direction for PGA corresponding to (a) 0.1 g, (b) 0.4 g, (c) 0.6 g, (d) 1.2 g.

In the transverse direction, the PFA distributions, not reported here for brevity reasons, show a similar trend. However, since the same level of IDR (i.e., damage) is attained in the transverse direction for lower PGAs with respect to the longitudinal one, the effect of nonlinearities on the PFA distribution (reduction of ratio PFA/PGA) is more evident starting from lower intensities.

Figure 11 shows the trend of maximum IDRs (a, b) and PFAs (c, d), respectively, for increasing seismic intensities (PGA). For each intensity, the value is obtained as maximum median value occurred at the different stories for both IDRs and PFAs. Observing Figure 11a, it is interesting to note that while for $PGA < 0.5\text{ g}$ the backbone curve by DR and BR predicts very similar IDRs, for $PGA \geq 0.5\text{ g}$ this phenomenon occurs for DR and

HG. Further, DR and HG distances from BR prediction as PGA increases up to $\text{PGA} = 1.5 \text{ g}$ where $\text{IDR}_{\max, \text{DR}} / \text{IDR}_{\max, \text{BR}}$ is almost 1.5. Similarly, this phenomenon can be also observed in the transverse direction (Figure 11b), despite $\text{PGA} \geq 0.57 \text{ g}$ predictions by DR and HG tend to diverge.

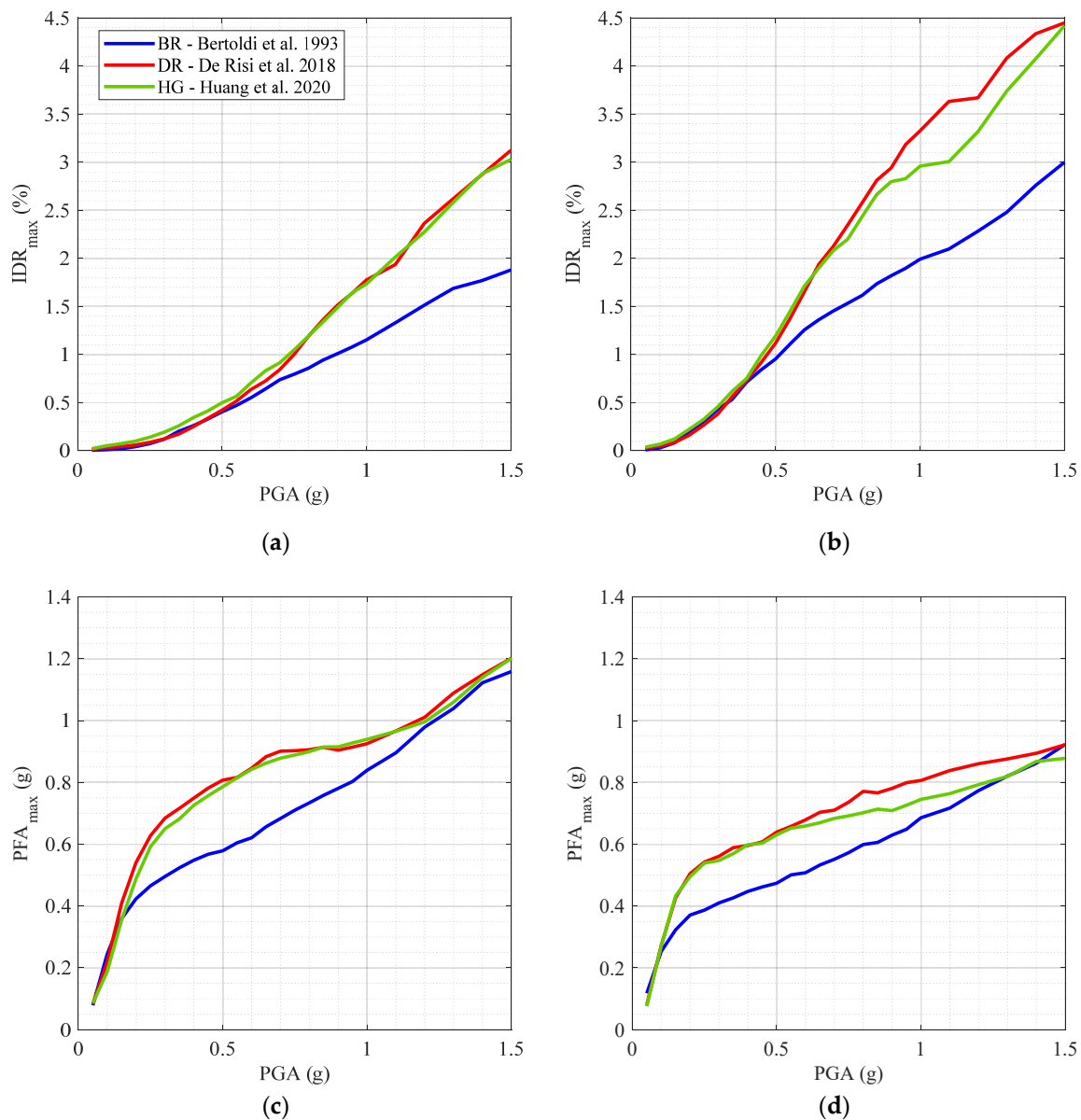


Figure 11. Maximum interstory drift ratios for (a) longitudinal and (b) transverse direction and maximum peak floor accelerations for (c) longitudinal and (d) transverse direction.

In the longitudinal direction (Figure 11c), three backbone curves predict similar PFA_{\max} up to $\text{PGA} = 0.15 \text{ g}$. While DR and HG produce PFA_{\max} very close to each other for every intensity, for $\text{PGA} \geq 0.15 \text{ g}$ they distance from BR for joining up again for $\text{PGA} \geq 1.2 \text{ g}$. This trend occurs also in the transverse direction (Figure 11d), but DR and HG predictions tend to diverge for $\text{PGA} \geq 0.5 \text{ g}$.

7. Conclusions

This paper investigates the influence of the models adopted for masonry infill panels on the global performance of RC frames. To this end, nonlinear static and time-history analyses are performed on a refined three-dimensional model where the infills are modeled

alternatively adopting truss elements with backbone curves proposed by Bertoldi et al. [37] (BR), De Risi et al. [48] (DR) and Huang et al. [49] (HG).

The main findings can be resumed in the following points:

- The presence of infills has a significant effect on the global response of RC frames both in terms of lateral stiffness and strength. This effect depends on the relative contribution to the lateral strength of the infill panels with respect to that of the RC frame and reduces as the opening percentage increases. For fully filled frames, the base shear strength increases between 227% and 365% with respect to that obtained for the corresponding bare frame configuration. The infill contribution reduces to a value comprised between 152% and 261% considering the actual opening configuration for the case-study building.
- The adopted constitutive model significantly influences the probability of attainment of a given damage state. The scatter in prediction between different constitutive models in terms of median PGAs is comprised between 2% and 60% depending on the adopted constitutive model and the selected damage state. The dispersion of results, which is related only to record-to-record variability, is slightly influenced by the constitutive law adopted while it mainly depends on the selected damage state and is comprised between 0.21 and 0.51 in terms of logarithmic dispersion.
- In terms of interstory drift ratios, the presence of infills lead to a more uniform distribution along the height with respect to the corresponding bare frame. For lower seismic intensities, a uniform distribution of lateral deformations along the height occurs, and the scatter of IDR due to different infill constitutive models may be very high and comprised between 270% and 590%. For increasing intensities, the scatter due to different infill constitutive models significantly lowers to values comprised between 4% and 56%. However, the distribution of lateral deformation shape along the height is not influenced by the employed constitutive model.
- In terms of peak floor accelerations, the distribution linearly increases along the height for lower seismic intensities. As the seismic intensity increases and the damage spreads throughout the structure, the acceleration demand reduces in upper stories with respect to the base acceleration. For higher seismic intensities, as the damage attained is very high, the acceleration demand at upper stories is lower than the base acceleration.

The results obtained in this study emphasize the effect of the selected infill constitutive model on the seismic performances of RC buildings. Although the study refers to a specific case-study building, the results may be useful to highlight relevant trends on the response and effects of relative infills model stiffness and strength on the evaluation of building damage fragility curves and performance evaluation. Future studies should analyze the dependence of the seismic performances of infilled RC frames on the other modeling assumptions, such as the adopted cyclic law and the dependence on the formulation to account for the presence of openings.

Author Contributions: M.G.d. and M.P. collected scientific articles for state of the art. M.G.d. performed the analyses, analyzed the results and contributed to write the paper. M.P. organized the work and contributed to the analyses of the results. A.P. revised the paper for overall consistency and scopes. All authors have read and agreed to the published version of the manuscript.

Funding: This research received no external funding.

Data Availability Statement: The data presented in this study are available on request from the corresponding author. The data are not publicly available due to privacy reasons.

Acknowledgments: This study was performed in the framework of PE 2019–2021 joint program DPC-Reluis–subproject WP2: Inventory of existing building typologies and WP4: Risk maps and seismic damage scenarios.

Conflicts of Interest: The authors declare no conflict of interest.

References

1. Polese, M.; Gaetani d'Aragona, M.; Prota, A. Simplified approach for building inventory and seismic damage assessment at the territorial scale: An application for a town in southern Italy. *Soil Dyn. Earthq. Eng.* **2019**, *121*, 405–420. [[CrossRef](#)]
2. Polese, M.; Di Ludovico, M.; Gaetani d'Aragona, M.; Prota, A.; Manfredi, G. Regional vulnerability and risk assessment accounting for local building typologies. *Int. J. Disaster Risk Reduct.* **2020**, *43*, 101400. [[CrossRef](#)]
3. Manfredi, G.; Prota, A.; Verderame, G.M.; De Luca, F.; Ricci, P. Emilia earthquake, Italy: Reinforced concrete buildings re-sponse. *Bull. Earthq. Eng.* **2014**, *12*, 2275–2298. [[CrossRef](#)]
4. Ricci, P.; Verderame, G.M.; Manfredi, G. Analytical investigation of elastic period of infilled RC MRF buildings. *Eng. Struct.* **2011**, *33*, 308–319. [[CrossRef](#)]
5. Gaetani d'Aragona, M.; Polese, M.; Prota, A. Influence Factors for the Assessment of Maximum Lateral Seismic Deformations in Italian Multistorey RC Buildings. In Proceedings of the 6th ECCOMAS Thematic Conference on Computational Methods in Structural Dynamics and Earthquake Engineering, Rhodes Island, Greece, 15–17 June 2017.
6. Gaetani d'Aragona, M.; Polese, M.; Cosenza, E.; Prota, A. Simplified assessment of maximum interstorey drift for RC buildings with irregular infills distribution along the height. *Bull. Earthq. Eng.* **2019**, *17*, 707–736. [[CrossRef](#)]
7. Dolšek, M.; Fajfar, P. The effect of masonry infills on the seismic response of a four storey reinforced concrete frame—A deterministic assessment. *Eng. Struct.* **2008**, *30*, 1991–2001. [[CrossRef](#)]
8. Penava, D.; Sarhosis, V.; Kožar, I.; Guljaš, I. Contribution of RC columns and masonry wall to the shear resistance of masonry infilled RC frames containing different in size window and door openings. *Eng. Struct.* **2018**, *172*, 105–130. [[CrossRef](#)]
9. Uva, G.; Porco, F.; Fiore, A. Appraisal of masonry infill walls effect in the seismic response of RC framed buildings: A case study. *Eng. Struct.* **2012**, *34*, 514–526. [[CrossRef](#)]
10. Tesfamariam, S.; Goda, K.; Mondal, G. Seismic vulnerability of reinforced concrete frame with unreinforced masonry infill due to mainshock–aftershock earthquake sequences. *Earthq. Spectra* **2015**, *31*, 1427–1449. [[CrossRef](#)]
11. Polese, M.; Gaetani d'Aragona, M.; Prota, A.; Manfredi, G. Seismic behavior of damaged buildings: A comparison of static and dynamic nonlinear approach. In Proceedings of the 4th ECCOMAS Thematic Conference on Computational Methods in Structural Dynamics and Earthquake Engineering, Kos Island, Greece, 12–14 June 2013; pp. 608–625.
12. Gaetani d'Aragona, M.; Polese, M.; Prota, A. Relationship between the variation of seismic capacity after damaging earthquakes, collapse probability and repair costs: Detailed evaluation for a non-ductile building. In Proceedings of the 5th ECCOMAS Thematic Conference on Computational Methods in Structural Dynamics and Earthquake Engineering, Crete Island, Greece, 25–27 May 2015; pp. 1478–1495.
13. Gaetani d'Aragona, M.; Polese, M.; Elwood, K.J.; Baradaran Shoraka, M.; Prota, A. Aftershock collapse fragility curves for non-ductile RC buildings: A scenario-based assessment. *Earthq. Eng. Struct. Dyn.* **2017**, *46*, 2083–2102. [[CrossRef](#)]
14. Ricci, P.; De Luca, F.; Verderame, G.M. 6th April 2009 L'Aquila earthquake, Italy: Reinforced concrete building performance. *Bull. Earthq. Eng.* **2011**, *9*, 285–305. [[CrossRef](#)]
15. Cavaleri, L.; Di Trapani, F. Prediction of the additional shear action on frame members due to infills. *Bull. Earthq. Eng.* **2015**, *13*, 1425–1454. [[CrossRef](#)]
16. Cavaleri, L.; Di Trapani, F.; Asteris, P.G.; Sarhosis, V. Influence of column shear failure on pushover based assessment of masonry infilled reinforced concrete framed structures: A case study. *Soil Dyn. Earthq. Eng.* **2017**, *100*, 98–112. [[CrossRef](#)]
17. Basha, S.H.; Kaushik, H.B. A novel macromodel for prediction of shear failure in columns of masonry infilled RC frames under earthquake loading. *Bull. Earthq. Eng.* **2019**, *17*, 2219–2244. [[CrossRef](#)]
18. Di Trapani, F.; Macaluso, G.; Cavaleri, L.; Papia, M. Masonry infills and RC frames interaction: Literature overview and state of the art of macromodeling approach. *Eur. J. Environ. Civ. Eng.* **2015**, *19*, 1059–1095. [[CrossRef](#)]
19. Noh, N.M.; Liberatore, L.; Mollaioli, F.; Tesfamariam, S. Modelling of masonry infilled RC frames subjected to cyclic loads: State of the art review and modelling with OpenSees. *Eng. Struct.* **2017**, *150*, 599–621. [[CrossRef](#)]
20. Gaetani d'Aragona, M.; Polese, M.; Di Ludovico, M.; Prota, A. Seismic vulnerability for RC infilled frames: Simplified evaluation for as-built and retrofitted building typologies. *Buildings* **2018**, *8*, 137. [[CrossRef](#)]
21. Polese, M.; Gaetani d'Aragona, M.; Di Ludovico, M.; Prota, A. Sustainable selective mitigation interventions towards effective earthquake risk reduction at the community scale. *Sustainability* **2018**, *10*, 2894. [[CrossRef](#)]
22. Asteris, P.G. Finite Element Micro-Modeling of Infilled Frames. *Elect. J. Struct. Eng.* **2008**, *8*, 1–11.
23. Asteris, P.; Cotsovou, D.; Chrysostomou, C.; Mohebbkhah, A.; Al-Chaar, G. Mathematical micromodeling of infilled frames: State of the art. *Eng. Struct.* **2013**, *56*, 1905–1921. [[CrossRef](#)]
24. Crisafulli, F. *Seismic Behavior of Reinforced Concrete Structures with Masonry Infills*; University of Canterbury: Canterbury, UK, 1997.
25. Crisafulli, F.J.; Carr, A.J.; Park, R. Analytical modelling of infilled frame structures—A general review. *Bull. N. Z. Soc. Earthq. Eng.* **2000**, *33*, 30–47.
26. Asteris, P.G.; Antoniou, S.T.; Sophianopoulos, D.S.; Chrysostomou, C.Z. Mathematical Macromodeling of Infilled Frames: State of the Art. *J. Struct. Eng.* **2011**, *137*, 1508–1517. [[CrossRef](#)]
27. Lourenço, P.B. Computations on historic masonry structures. *Prog. Struct. Eng. Mater.* **2002**, *4*, 301–319. [[CrossRef](#)]
28. Asteris, P.; Tzamtzis, A. On the use of a regular yield surface for the analysis of unreinforced masonry walls. *Electron. J. Struct. Eng.* **2003**, *3*, 23–42.
29. Stafford Smith, B. Behaviour of square infilled frames. *J. Struct. Div.* **1966**, *92*, 381–403. [[CrossRef](#)]

30. Mainstone, R.J. On the stiffness and strength of infilled frames. In Proceedings of the Institute of Civil Engineers, London, UK, June 1971; Volume 7360S, pp. 57–89. [\[CrossRef\]](#)
31. Mainstone, R.J. *Supplementary Note on the Stiffness and Strength of Infilled Frames Current Paper CP 13/UK: Building Research Establishment*; Building Research Station: Watford, UK, 1974.
32. Holmes, M. Steel frames with brickwork and concrete filling. In Proceedings of the Institution of Civil Engineers, London, UK, August 1961; Volume 19, pp. 473–478. [\[CrossRef\]](#)
33. Chrysostomou, C.Z.; Gergely, P.; Abel, J.F. A six-strut model for nonlinear dynamic analysis of steel infilled frames. *Int. J. Struct. Stab. Dyn.* **2002**, *2*, 335–353. [\[CrossRef\]](#)
34. El-Dakhkhni, W.W.; Elgaaly, M.; Hamid, A.A. Three-Strut Model for Concrete Masonry-Infilled Steel Frames. *J. Struct. Eng.* **2003**, *129*, 177–185. [\[CrossRef\]](#)
35. Combescure, D. Some contributions of physical and numerical modelling to the assessment of existing masonry infilled RC frames under extreme loading. In Proceedings of the First European Conference on Earthquake Engineering and Seismology, Geneva, Switzerland, 3–8 September 2006.
36. Verderame, G.M.; De Luca, F.; Ricci, P.; Manfredi, G. Preliminary analysis of a soft-storey mechanism after the 2009 L’Aquila earthquake. *Earthq. Eng. Struct. Dyn.* **2011**, *40*, 925–944. [\[CrossRef\]](#)
37. Bertoldi, S.H.; Decanini, L.D.; Gavarini, C. Telai tamponati soggetti ad azioni sismiche, un modello semplificato: Confronto sperimentale e numerico. In Proceedings of the 6 Convegno Nazionale L’ingegneria Sismica in Italia, Perugia, Italy, 13–15 October 1993.
38. Panagiotakos, T.B.; Fardis, M.N. Seismic response of infilled RC frames structures. In Proceedings of the 11th World Conference on Earthquake Engineering, Acapulco, Mexico, 23–28 June 1996.
39. Asteris, P.G.; Cavaleri, L.; Di Trapani, F.; Sarhosis, V. A macro-modelling approach for the analysis of infilled frame structures considering the effects of openings and vertical loads. *Struct. Infrastruct. Eng.* **2016**, *12*, 551–566. [\[CrossRef\]](#)
40. Zarnic, R.; Tomazevic, M. Study of the behaviour of masonry infilled reinforced concrete frames subjected to seismic loading. In Proceedings of the Seventh International Brick Masonry Conference, Melbourne, Australia, 17–20 February 1985; Volume 2, pp. 1315–1325.
41. Zarnic, R.; Tomazevic, M. An experimentally obtained method for evaluation of the behaviour of masonry infilled R/C frames. In Proceedings of the Ninth World Conference on Earthquake Engineering, Tokyo, Japan, 2–6 August 1988; Volume VI, pp. 163–168.
42. Polyakov, S. On the interaction between masonry filler walls and enclosing frame when loading in the plane of the wall. *Transl. Earthq. Eng.* **1960**, *E2*, 36–42.
43. Liauw, T.C.; Kwan, K. Nonlinear behaviour of non-integral infilled frames. *Comput. Struct.* **1984**, *18*, 551–560.
44. Decanini, L.D.; Fantin, G.E. Modelos Simplificados de la Mamposteria Incluida en Porticos. Características de Rigidez y Resistencia Lateral en Estrado Limite (in Spanish). *J. Argent. Ing. Estruct.* **1987**, *2*, 817–836.
45. Dawe, J.L.; Seah, C.K. Analysis of concrete masonry infilled steel frames subjected to in-plane loads. In Proceedings of the 5th Canadian Masonry Symposium, Vancouver, BC, Canada, 5–7 June 1989; pp. 329–340.
46. Durrani, A.J.; Luo, Y.H. Seismic retrofit of flat-slab buildings with masonry infill. In Proceedings of the NCEER Workshop on Seismic Response of Masonry Infills, San Francisco, CA, USA, 4–5 February 1994; Report NCEER-94-0004.
47. Saneinejad, A.; Hobbs, B. Inelastic Design of Infilled Frames. *J. Struct. Eng.* **1995**, *121*, 634–650. [\[CrossRef\]](#)
48. De Risi, M.T.; Del Gaudio, C.; Ricci, P.; Verderame, G.M. In-plane behaviour and damage assessment of masonry infills with hollow clay bricks in RC frames. *Eng. Struct.* **2018**, *168*, 257–275. [\[CrossRef\]](#)
49. Huang, H.; Burton, H.V.; Sattar, S. Development and Utilization of a Database of Infilled Frame Experiments for Numerical Modeling. *J. Struct. Eng.* **2020**, *146*, 04020079. [\[CrossRef\]](#)
50. De Sortis, A.; Bazzurro, P.; Mollaioli, F.; Bruno, S. Influenza delle tamponature sul rischio sismico degli edifici in calcestruzzo armato. In Proceedings of the ANIDIS Conference L’ingegneria Sismica in Italia, Pisa, Italy, 10–14 June 2007. (In Italian).
51. Mosalam, K.M.; White, R.N.; Gergely, P. Static Response of Infilled Frames Using Quasi-Static Experimentation. *J. Struct. Eng.* **1997**, *123*, 1462–1469. [\[CrossRef\]](#)
52. Al-Chaar, G.; Lamb, G.E.; Issa, M.A. Effects of openings on structural performance of unreinforced masonry infilled frames. In *Large Scale Structural Testing*; Issa, M.A., Ed.; ACI Spec. Publ: Washington, DC, USA, 2003; Volume 211, pp. 247–262.
53. Mohammadi, M.; Nikfar, F. Strength and Stiffness of Masonry-Infilled Frames with Central Openings Based on Experimental Results. *J. Struct. Eng.* **2013**, *139*, 974–984. [\[CrossRef\]](#)
54. Decanini, L.D.; Liberatore, L.; Mollaioli, F. Strength and stiffness reduction factors for infilled frames with openings. *Earthq. Eng. Eng. Vib.* **2014**, *13*, 437–454. [\[CrossRef\]](#)
55. Basha, S.H.; Surendran, S.; Kaushik, H.B. Empirical Models for Lateral Stiffness and Strength of Masonry-Infilled RC Frames Considering the Influence of Openings. *J. Struct. Eng.* **2020**, *146*, 04020021. [\[CrossRef\]](#)
56. Klingner, R.E.; Bertero, V.V. Earthquake resistance of infilled frames. *J. Struct. Div.* **1978**, *104*, 973–989. [\[CrossRef\]](#)
57. Cavaleri, L.; Fossetti, M.; Papia, M. Infilled frames: Developments in the evaluation of cyclic behaviour under lateral loads. *Struct. Eng. Mech.* **2005**, *21*, 469–494. [\[CrossRef\]](#)
58. Cavaleri, L.; Di Trapani, F. Cyclic response of masonry infilled RC frames: Experimental results and simplified modeling. *Soil Dyn. Earthq. Eng.* **2014**, *65*, 224–242. [\[CrossRef\]](#)

59. Tassios, T.P. *Masonry Infill and RC Walls under Cyclic Actions, Proceedings of the 3rd International Symposium on Wall Structures, Warsaw, Poland, 1984*; CIB: Ottawa, ON, Canada, 1984.
60. Crisafulli, F.J.; Carr, A.J. Proposed macro-model for the analysis of infilled frame structures. *Bull. N. Z. Soc. Earthq. Eng.* **2007**, *40*, 69–77. [[CrossRef](#)]
61. Lowes, L.N.; Mitra, N.; Altoontash, A. *A Beam-Column Joint Model for Simulating the Earthquake Response of Reinforced Concrete Frames*; Technical Rep. No. PEER 2003/10; Pacific Earthquake Engineering Research Center: Berkeley, CA, USA, 2003.
62. Jeon, J.-S.; Park, J.-H.; Desroches, R. Seismic fragility of lightly reinforced concrete frames with masonry infills. *Earthq. Eng. Struct. Dyn.* **2015**, *44*, 1783–1803. [[CrossRef](#)]
63. Lima, C.; De Stefano, G.; Martinelli, E. Seismic response of masonry infilled RC frames: Practice-oriented models and open issues. *Earthq. Struct.* **2014**, *6*, 409–436. [[CrossRef](#)]
64. Koutromanos, I.; Stavridis, A.; Shing, P.B.; Willam, K. Numerical modeling of masonry-infilled RC frames subjected to seismic loads. *Comput. Struct.* **2011**, *89*, 1026–1037. [[CrossRef](#)]
65. Kumar, M.; Rai, D.C.; Jain, S.K. Ductility Reduction Factors for Masonry-Infilled Reinforced Concrete Frames. *Earthq. Spectra* **2015**, *31*, 339–365. [[CrossRef](#)]
66. Kakaletsis, D.J.; Karayannis, C.G. Influence of Masonry Strength and Openings on Infilled R/C Frames under Cycling Loading. *J. Earthq. Eng.* **2008**, *12*, 197–221. [[CrossRef](#)]
67. Ricci, P.; De Risi, M.T.; Verderame, G.M.; Manfredi, G. Influence of infill distribution and design typology on seismic performance of low-and mid-rise RC buildings. *Bull. Earthq. Eng.* **2013**, *11*, 1585–1616. [[CrossRef](#)]
68. Gaetani d’Aragona, M.; Polese, M.; Di Ludovico, M.; Prota, A. The use of Stick-IT model for the prediction of direct economic losses. *Earthq. Eng. Struct. Dyn.* **2020**. [[CrossRef](#)]
69. Gaetani d’Aragona, M.; Polese, M.; Prota, A. Stick-IT: A simplified model for rapid estimation of IDR and PFA for existing low-rise symmetric infilled RC building typologies. *Eng. Struct.* **2020**, *223*, 111182. [[CrossRef](#)]
70. Hak, S.; Morandi, P.; Magenes, G.; Sullivan, T.J. Damage Control for Clay Masonry Infills in the Design of RC Frame Structures. *J. Earthq. Eng.* **2012**, *16*, 1–35. [[CrossRef](#)]
71. FEMA 356. *Prestandard and Commentary for the Seismic Rehabilitation of Buildings*; Federal Emergency Management Agency: Washington, DC, USA, 2000.
72. Ministero delle Infrastrutture e dei Trasporti. In *Proceedings of the Circolare n.7 C.S.LL.PP 21 January 2019 Istruzioni per L’applicazione dell’Aggiornamento delle Norme Tecniche per le Costruzioni di cui al Decreto Ministeriale 17 gennaio 2018*; Ministero delle Infrastrutture e dei Trasporti, C.S.LL.PP: Rome, Italy, 2019. (In Italian)
73. Liberatore, L.; Noto, F.; Mollaioli, F.; Franchin, P. In-plane response of masonry infill walls: Comprehensive experimentally-based equivalent strut model for deterministic and probabilistic analysis. *Eng. Struct.* **2018**, *167*, 533–548. [[CrossRef](#)]
74. Applied Technology Council & United States. *Quantification of Building Seismic Performance Factors—FEMA P695*; US Department of Homeland Security: Washington, DC, USA, 2009.
75. Baker, J.W. Efficient Analytical Fragility Function Fitting Using Dynamic Structural Analysis. *Earthq. Spectra* **2015**, *31*, 579–599. [[CrossRef](#)]
76. Grunthal, G. *Cahiers du Centre Européen de Géodynamique et de Séismologie*; European Macroseismic Scale: Luxembourg, 1998; pp. 1–97.
77. Del Gaudio, C.; Ricci, P.; Verderame, G.M. A class-oriented mechanical approach for seismic damage assessment of RC buildings subjected to the 2009 L’Aquila earthquake. *Bull. Earthq. Eng.* **2018**, *16*, 4581–4605. [[CrossRef](#)]
78. Porter, K.A. An overview of PEER’s performance-based earthquake engineering methodology. In *Proceedings of the 9th Inter-National Conference on Applications of Statistics and Probability in Civil Engineering*, Francisco, CA, USA, 6–9 July 2003.